Reaction rate for $^{31}S(p,\gamma)^{32}Cl$ and its influence on the SiP cycle in hot stellar hydrogen burning

S. Vouzoukas, C.P. Browne, U. Giesen,* J. Görres, S.M. Graff, H. Herndl,† C. Iliadis,* L.O. Lamm,‡ J. Meissner, J.G. Ross,§ K. Scheller,‖ L. van Wormer,¶ and M. Wiescher
Department of Physics, University of Notre Dame, Notre Dame, Indiana 46556

A.A. Rollefson
Department of Physics and Astronomy, University of Arkansas, Little Rock, Arkansas 72204
(Received 15 December 1993)

The excitation energies of the proton unbound states in ^{32}Cl have been measured in the $^{32}S(^3He,t)^{32}Cl$ charge exchange reaction with high accuracy. The partial widths of the unbound levels have been calculated to derive the resonance strengths of these states in the $^{31}S(p,\gamma)^{32}Cl$ reaction channel. The reaction rate for the $^{31}S(p,\gamma)^{32}Cl$ reaction has been calculated and is compared with previous estimates. The role of this reaction for the closure of the SiP cycle is discussed in terms of the temperature and density conditions in hot stellar hydrogen burning.

PACS number(s): 25.55.Kr, 25.40.Lw, 97.10.Cv, 27.30.+t

I. INTRODUCTION

The rapid proton capture (rp) process has been identified as the dominant nucleosynthesis process in explosive hydrogen burning [1] expected for example in novae and x-ray bursts. Light mass material (C, N, O, Ne) will be processed by a series of proton capture reactions and β-decays towards the Fe-Ni region. The characteristic time scale for this process τ_{tot} is determined by the sum of the lifetimes for β decay, τ_β, and proton capture, $\tau_{(p,\gamma)}$, of the isotopes along the main process path,

$$\tau_{tot} = \sum_i \tau_i = \sum_i \left[\tau_{\beta_i} + \tau_{(p,\gamma)_i}\right], \tag{1}$$

with $\tau_{(p,\gamma)} = (Y_H \rho N_A \langle\sigma v\rangle)^{-1} = \left(\lambda_{(p,\gamma)}\right)^{-1}$. Y_H is the hydrogen abundance and ρ is the stellar density. The main delays for the process are long β-decay times and small proton capture rates. An additional impedance, however, is caused by cyclic reaction sequences [2]. This may take place if the α threshold is lower than the proton threshold in the compound nucleus of a proton capture reaction along the rp-process path. In these cases the cycle may be closed by a (p,α) reaction (consider the NeNa-, SiP-, SCl-cycle, etc.) and nuclear material is stored in the cycle for a certain period of time τ_{cycl}. This will cause a temporary enrichment of the abundances of the isotopes within the cycle which can only be depleted by breakout or leakage reactions. The dominant leakage reaction at lower temperature conditions is the (p,γ) reaction competing with the (p,α) reaction. This reaction branching, e.g., $^{23}Na\ (p,\gamma)/(p,\alpha)$ in the NeNa cycle, and $^{31}P(p,\gamma)/(p,\alpha)$ in the SiP cycle, determines the storage time τ_{cycl},

$$\tau_{cycl} = \frac{\lambda_{(p,\alpha)} + \lambda_{(p,\gamma)}}{\lambda_{(p,\gamma)}} \left[\sum_j \tau_j^c\right], \tag{2}$$

where τ_j^c are the lifetimes of the isotopes in the reaction cycle and $\lambda_{(p,\gamma)}$ and $\lambda_{(p,\alpha)}$ are the reaction rates for the (p,γ) and (p,α) reactions. For higher temperature scenarios a breakout may also occur by a proton capture on a long-lived isotope in the cycle, e.g., $^{23}Mg(p,\gamma)$, $^{27}Si(p,\gamma)$, $^{31}S(p,\gamma)$, etc. This alters the storage time in the cycle to

$$\tau_{cycl} = \left(\frac{\lambda_{(p,\gamma)}}{\lambda_{(p,\alpha)} + \lambda_{(p,\gamma)}} + \frac{\lambda'_{(p,\gamma)}}{\lambda_\beta + \lambda'_{(p,\gamma)}}\right)^{-1} \left[\sum_j \tau_j^c\right], \tag{3}$$

where $\lambda'_{(p,\gamma)}$ is the reaction rate for the proton capture on the β–unstable-but-"long-lived" isotope with a β-decay rate of λ_β. It is clear that large break out rates limit the storage time to the sum of the lifetimes of the isotopes in the cycle. For small leakage rates the storage time becomes large, eventually larger than the macroscopic time scale of the hot hydrogen-burning scenario. In this case the cycle would be the end point of the rp-process nucleosynthesis and the equilibrium abundance distribution in the cycle would reflect the final nucleosynthesis abundance distribution. This should be observable in the isotopic abundance distribution of the ejected material.

*Present address: TRIUMF, Vancouver, Canada.
†Permanent address: Technische Universität Wien, Institut für Kernphysik, Wien, Austria.
‡Present address: Presbyterian College, Clinton, SC 29325.
§Present address: University of Central Arkansas, Conway, AR 72032.
‖Present address: University of Evansville, Evansville, IN 47701.
¶Present address: Hiram College, Hiram, OH 44234.

While the reaction rates in the (p,γ), (p,α) branchings have been extensively studied in recent years [3–6], only limited information is available about the reaction rates for proton capture on the unstable $T_z = -1/2$ nuclei ^{23}Mg, ^{27}Si, and ^{31}S. The reaction rates for ^{23}Mg$(p,\gamma)^{24}$Al and ^{27}Si$(p,\gamma)^{28}$P have been estimated earlier [7]; however, considerable uncertainty exists about the influence of the ^{31}S$(p,\gamma)^{32}$Cl reaction rate on the closure of the SiP cycle. This cycle may be of particular importance for the nucleosynthesis in novae as recent observations [8–11] indicate large overabundances of Si and S in the ejecta. This may have been caused by an enrichment process in the SiP cycle as just described.

In the present work we attempted to determine the excitation energies of the proton unbound states in ^{32}Cl with high accuracy. These states may contribute as resonances to the ^{31}S(p,γ) reaction channel and will determine the reaction rate. We measured the ^{32}S(^{3}He,t)^{32}Cl charge exchange reaction using the broad range spectrograph at the University of Notre Dame. We then compare the present results with those of a recent study of ^{32}S(^{3}He,t)^{32}Cl [12] and those of measurements of the β-delayed proton decay of ^{32}Ar [13–15]. Finally, we discuss the influence of the observed levels on the stellar reaction rate of ^{31}S$(p,\gamma)^{32}$Cl and evaluate its impact on the closure of the SiP cycle.

II. EXPERIMENTAL PROCEDURES AND RESULTS

The experiment was performed with the FN-Tandem accelerator and the 100 cm broad-range magnetic spectrograph [16] at the Nuclear Structure Laboratory of the University of Notre Dame. The ^{32}S(^{3}He,t)^{32}Cl reaction ($Q = -12.706$ MeV) was investigated at various ^{3}He beam energies between 22.5 and 25 MeV with beam intensities ranging between 0.1 and 0.5 particle μA on target. Because of the small reaction cross section and the relatively small solid angle of the spectrograph, data were taken only at forward angles, $7.5° \leq \Theta_{\rm lab} \leq 20°$. Different targets have been used in the course of the experiments. Originally, thick targets ($\approx$650 μg/cm^2) were produced by evaporating CdS onto 10 to 20 μg/cm^2 carbon foils. A typical triton spectrum obtained with one of these thick targets is shown in Fig. 1. Note the poor energy resolution of $\approx$ 40 keV due primarily to energy straggle within the target. In addition, the rather large energy losses within the target lead to sizeable uncertainties ($\approx$ 20 keV) in the determination of excitation energies. Based on the results of these initial experiments, a technique was developed to produce thinner targets via implantation. The Notre Dame SNICS ion source was used to implant 70 keV ^{32}S$^-$ ions into 40 μg/cm^2 carbon foils. The carbon foils were light flashed with a xenon strobe from a distance of approximately 25 cm prior to implantation. This procedure relaxes the initial foil tension and prevents the fracture of the foil during implantation.

A carbon collimator placed between the ion source and the target foil served to replace the carbon sputtered from the foil by the ^{32}S$^-$ beam, and to create a protective carbon layer which prevented the beam from sputtering away any ^{32}S already implanted in the foil [17]. A typical triton spectrum obtained using these thinner implanted targets is shown in Fig. 2. The substantial improvement in the energy resolution is obvious from the figure, and the small energy loss within these thin foils leads to a significant reduction in the uncertainty of the determination of the excitation energies. While both the thicker CdS targets and the thinner implanted targets were used in the course of the experiments, the excitation energies

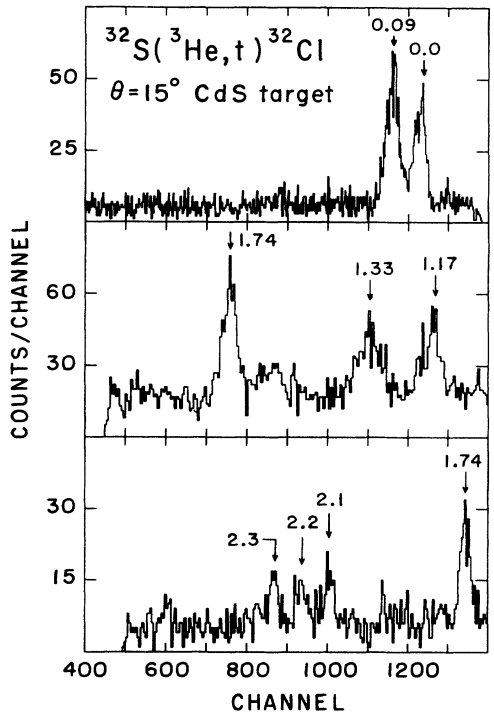

FIG. 1. A set of typical ^{32}S(^{3}He,t)^{32}Cl triton spectra covering the excitation range in ^{32}Cl up to 2.5 MeV. The data were obtained with a thick CdS target at an angle of $\Theta = 15°$.

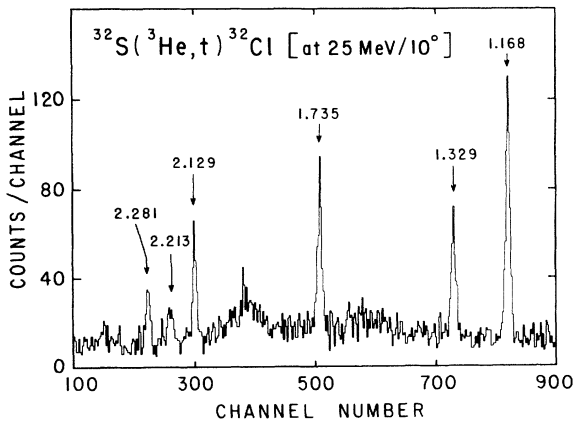

FIG. 2. A ^{32}S(^{3}He,t)^{32}Cl triton spectrum measured at $\Theta = 10°$ with an implanted ^{32}S target.

of the observed levels in ^{32}Cl were determined only from the data obtained from the implanted targets. The exceptions to this are the ground state and the first excited state, which were observed using CdS targets but were not investigated using the implanted targets.

The reaction products were detected at the focal surface of the spectrograph using a position-sensitive proportional gas counter system backed with a plastic scintillator [18]. This detector gives position, energy loss, and total energy signals for the reaction products, from which particle momentum and identification are determined. A calibration of the position signal was determined using 25 MeV ^3He particles elastically scattered from a thin Au foil, measured in reflection at $\Theta_{lab} = 70°$ with the target at an angle of 35° with respect to the beam direction. The ^3He beam energy was verified using photographic emulsion track-plate detection for which an absolute calibration of the spectrograph is known.

The level structure of ^{32}Cl was studied from the ground state to excitation energies of $\approx$ 2.5 MeV, using the thicker CdS targets. Since the detector covers only a limited section of the focal plane, the data were taken in three overlapping momentum ranges. A total of eight levels (including the ground state) were observed. The spectra shown in Fig. 1 were taken at $\Theta_{lab} = 15°$ with a 22.5 MeV ^3He beam incident upon a thick CdS target. As previously noted, the poor energy resolution prevents an accurate determination of the level energies, and the peaks are therefore labeled with only the approximate excitation energies. The spectrum in Fig. 2 was taken at $\Theta_{lab} = 10°$ with a 25 MeV ^3He beam on an implanted ^{32}S target. The energy resolution was then limited primarily by the spread in the beam energy. The states of astrophysical interest were observed with a single magnetic field setting, chosen to include the well established $J^\pi = 1^+$ level at $E_x = 1.1685$ MeV [13]. In the kinematic analysis of the observed levels, excitation energies were measured relative to that of this well known state. Uncertainties in beam energy, reaction angle, and stopping in the target contribute a negligible amount to the total, with the major uncertainties arising from the determination of the centroids of the groups and from the calibration of position to pulse height. The weighted averages for the excitation energies of those levels observed with the implanted target are listed in Table I. The results of previous work are also listed, as are the compilation values [19]. The present excitation energies are in excellent agreement with the results of the β-delayed proton- and γ-decay measurements [13]. Good agreement with the results of previous (^3He,t) measurements [8] is obtained if their values are scaled relative to the known excitation energy of the 1.1685 MeV state. The compilation values do not agree with the present results, and there is some disagreement with the value of Schardt [14] for the 2.213 MeV state.

Table I also lists the excitation energy, spin, and parity for the known mirror states in ^{32}P. The spin assignments are based on the (^3He,t) angular distribution measurement [13] and on the log ft values determined in the β-decay measurements [13–15], which allow unambiguous analog assignments for the observed ^{32}Cl and the known ^{32}P levels.

III. PARTIAL WIDTHS OF THE OBSERVED LEVELS IN ^{32}Cl

The resonance strength $\omega\gamma$ of the observed ^{32}Cl unbound states in the $^{31}S(p,\gamma)^{32}Cl$ reaction channel can be calculated directly from the proton- and γ-partial widths, Γ_p and Γ_γ, respectively,

$$\omega\gamma = \frac{2J+1}{(2j_T+1)(2j_p+1)}\frac{\Gamma_p\Gamma_\gamma}{\Gamma_{tot}}. \quad (4)$$

The total width of the state can be determined from the partial widths, $\Gamma_{tot} = \Gamma_p + \Gamma_\gamma$, and J, j_p, and j_T are the spins of the resonance, projectile, and target nucleus ($j_p^\pi = j_T^\pi = 1/2^+$), respectively. The proton partial width can be calculated as a function of the penetrability through the Coulomb barrier $P_\ell(E_p)$ and the single particle spectroscopic factor C^2S of the resonance level,

$$\Gamma_p = 3\frac{\hbar^2}{\mu R^2}P_\ell(E)C^2S, \quad (5)$$

TABLE I. Excitation energies and spin and parities of the observed levels in ^{32}Cl and ^{32}P.

$^{32}S(^3He,t)^{32}Cl$			$^{32}Ar(\beta^+-\gamma,p)^{32}Cl,^{31}S$			^{32}P	
E_x (keV)		J^π	E_x (keV)	J^π	E_x (keV)	E_x (keV)	J^π
Present study	Jeanperrin[a]		Björnstad[b]		Schardt[c]	Endt[d]	
1168[e]	1157±5	1^+	1168.5±0.2	1^+		1150±3	1^+
1329±3	1326±5	2^+				1323±2	2^+
1735±3	1719±4	3^+				1755±10	3^+
2129±3	2122±7	$(3\text{-}5)^+$				2177±2	3^+
2213±3	2193±7	$(1,2)^+$	2201±20	1^+	2195±10	2230±6	1^+
2281±3	2270±5	$(1,2)^+$				2218±11	2^+
						2313±10	$(1\text{-}3)^+$

[a]Ref. [12].
[b]Ref. [13].
[c]Refs. [14,15].
[d]Ref. [19].
[e]Reference value.

with $R = 1.26(A_T^{1/3} + A_p^{1/3})$ fm as the nuclear channel radius, A_T and A_p are the target and projectile mass numbers and μ is the reduced mass. The γ partial width can be expressed in terms of the reduced transition probability $B(\Pi L)$ for the γ decay with the magnetic or electric multipolarity L and the γ-energy E_γ,

$$\Gamma_\gamma = \frac{8\pi(L+1)}{L[(2L+1)!!]^2}\left(\frac{E_\gamma}{\hbar c}\right)^{(2L+1)} B(\Pi L). \qquad (6)$$

The single particle spectroscopic factors and the reduced transition probabilities of the observed $T = 1$ levels in ^{32}Cl have been calculated in the standard shell model. The mass-dependent Wildenthal interaction was used, assuming a full *sd* shell space with a ^{16}O core. The spectroscopic factors are compared in Table II with the experimental data from the single particle transfer reaction studies, ^{31}P$(d,p)^{32}$P, to the mirror states in ^{32}P. The factors show excellent agreement for the 2^+ and 1^+ states. For the two 3^+ levels the theoretical values overestimate the experimental data by a factor of 2.3. The reduced transition strengths of the $M1$ and $E2$ γ transitions to the lower excited states have also been calculated. To compensate for the incompleteness of the truncated shell model space, effective proton and neutron charges of $e_p = 1.35e$ and $e_n = 0.35e$, respectively, were introduced for the calculation of the $E2$ strength. For the $M1$ transitions the matrix elements of Ref. [20] were used. The γ widths Γ_γ were calculated from the reduced transition strengths using Eq. (6). The γ widths for the different transitions were calculated for ^{32}Cl and the mirror nucleus ^{32}P as a sum of the $M1$ and $E2$ widths and are listed in Table III in comparison with the experimental γ widths for the corresponding transitions in the mirror nucleus ^{32}P. Table IV lists the center of mass energies of the expected resonances in ^{31}S$(p,\gamma)^{32}$Cl, which were calculated from the excitation energies in Table I for a reaction Q value of Q=1573±8 keV. Figure 3 shows the level scheme for the observed $T = 1$ states in ^{32}Cl, indicating the proton threshold and the resonance energies (in the lab system). Because of the large uncertainty in the reaction Q value, the resonance energies are uncertain by ±11 keV.

Table IV lists the resonance strengths derived by Eq. (4) from the experimental and theoretical input parameters, respectively. No attempt has been made to assign errors to the theoretical input parameters. The error of $\omega\gamma_{\text{theo}}$ reflects only the uncertainty of the resonance energy which influences the penetrability. This amounts to a factor of three uncertainty for the proton width of the resonance at E_r=162 keV and to an uncertainty between 20% and 30% for the proton widths of the higher energy resonances. The error of $\omega\gamma_{\text{expt}}$ includes in addition the experimental uncertainty of the lifetimes of the mirror levels in ^{32}P.

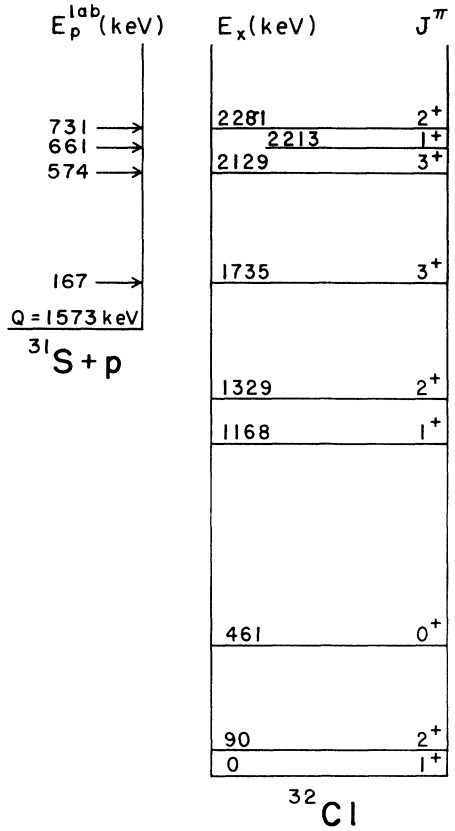

FIG. 3. Observed level sequence in ^{32}Cl. Also indicated are the energies of the expected resonances in ^{31}S$(p,\gamma)^{32}$Cl.

Except for the J^π=2^+ resonance at E_r=708 keV, good agreement within the overall uncertainties is observed. For the two J^π= 3^+ resonances at 162 and 556 keV the proton widths are considerably smaller than the γ partial widths due to the high Coulomb and angular momentum barriers. Therefore the resonance strength is determined by the proton partial width of the state. In the case of the two resonances at 640 keV (1^+) and 708 keV (2^+) the γ channel is much weaker than the proton-decay channel. The predicted resonance strengths therefore depend mainly on the γ partial widths.

For the following astrophysical considerations the reso-

TABLE II. Spectroscopic single particle factors for the observed $T = 1$ levels in ^{32}Cl and ^{32}P.

	^{32}Cl			^{32}P	
	Expt. values	Calc. values		Expt. values	
J^π	E_x (keV)	E_x (keV)	C^2S	E_x (keV)	C^2S
3^+	1735±3	1528	1.34×10^{-2}	1755±10	5.7×10^{-3}
3^+	2129±3	2223	6.60×10^{-3}	2177±2	2.9×10^{-3}
1^+	2213±3	1965	2.86×10^{-2}	2230±6	3.3×10^{-2}
2^+	2281±3	2036	3.23×10^{-2}	2218±11	3.0×10^{-2}

TABLE III. Experimental and theoretical γ widths for the transitions of the observed $T = 1$ levels in ^{32}Cl and ^{32}P.

	^{32}Cl			^{32}P	
	$\Gamma_\gamma(M1)$ (eV)	$\Gamma_\gamma(E2)$ (eV)	Γ_γ (eV)	Γ_γ (eV)	
Transition		Calc. values		Calc. values	Expt. values
$3_1 \rightarrow 1_1$		2.8×10^{-7}	2.8×10^{-7}	1.1×10^{-7}	2.1×10^{-5}
$3_1 \rightarrow 2_1$	5×10^{-5}	2.5×10^{-4}	3×10^{-4}	3.3×10^{-4}	9.6×10^{-4}
$3_2 \rightarrow 1_1$		4.7×10^{-4}	4.7×10^{-4}	8.9×10^{-4}	9.6×10^{-4}
$3_2 \rightarrow 2_1$	7.24×10^{-3}	1.3×10^{-4}	7.37×10^{-3}	1.05×10^{-2}	9.7×10^{-3}
$1_3 \rightarrow 1_1$	8.76×10^{-3}	1×10^{-5}	8.77×10^{-3}	6.57×10^{-3}	1.1×10^{-3}
$1_3 \rightarrow 2_1$	1.58×10^{-2}	1.3×10^{-4}	1.59×10^{-2}	1.9×10^{-2}	1.68×10^{-2}
$2_3 \rightarrow 1_1$	6×10^{-5}	5.1×10^{-4}	5.7×10^{-4}	3.2×10^{-4}	1.4×10^{-3}
$2_3 \rightarrow 2_1$	5.3×10^{-4}	1×10^{-5}	5.4×10^{-4}	1.7×10^{-3}	3.6×10^{-4}
$2_3 \rightarrow 1_2$	2.1×10^{-4}	1×10^{-5}	2.2×10^{-4}	2.3×10^{-4}	2.7×10^{-4}
$2_3 \rightarrow 2_2$	1.05×10^{-3}		1.05×10^{-3}	9×10^{-4}	9.6×10^{-4}

nance strengths based on the experimental input parameters have been chosen.

IV. ASTROPHYSICAL IMPLICATIONS

The stellar reaction rate of $^{31}S(p,\gamma)^{32}Cl$ is determined mainly by the resonant reaction contributions. To determine the resonant reaction component reliably, exact knowledge of the resonance energy E_r and the resonance strength $\omega\gamma$ is necessary (see Table IV). The reaction rate is expressed by [21]

$$N_A\langle\sigma v\rangle = 1.54\times10^{11}(\mu T_9)^{-3/2}\omega\gamma\exp\left[-\frac{11.605E_r}{T_9}\right] \tag{7}$$

in units of $cm^3\,s^{-1}\,mole^{-1}$, where μ is the reduced mass of the target-projectile system in atomic mass units, T_9 is the temperature in 10^9 K, and the resonance energy and strength are in units of MeV.

Figure 4 and Table V show the contribution of the single resonances as a function of temperature. The weak 3^+ resonance at 162 keV contributes only at low temperatures, $T_9 \leq 0.25$, while for higher temperatures the reaction rate is entirely dominated by the 3^+ resonance at 556 keV. At very high temperatures, $T_9 \geq 0.7$, the 1^+ resonance at 640 keV determines the total rate. The shaded areas in Fig. 4 indicate the uncertainties in the single resonant contributions, which are due to the uncertainties in the resonance energies and partial widths.

Figure 5 shows the ratio of the present rate and the estimated rate previously proposed and used by Wallace and Woosley [1]. The previous rate was based on the assumption of a weak resonance at 200 keV only. The figure indicates that the present rate is up to two orders of magnitude smaller in the temperature range $0.1 \leq T_9 \leq 0.4$. At higher temperatures the additional contributions of higher energy resonances increase the rate by up to four orders of magnitude compared to the previous estimate [1].

To evaluate the importance of the reaction for nucleosynthesis in the Si,P,S mass region the rate has to be compared with the β-decay rate of ^{31}S, which is in first approximation temperature and density independent ($T_{1/2} = 2.58$ s),

$$\lambda_\beta = \frac{\ln 2}{T_{1/2}}, \tag{8}$$

and with the rate of the inverse photodisintegration which may hinder the (p,γ) reaction substantially because of the fairly low reaction Q value. The inverse reaction rate can be calculated by detailed balance from the (p,γ)-rate,

$$\lambda_{(\gamma,p)} = 9.87\times10^9\mu^{3/2}T_9^{3/2}\omega^{-1}N_A\langle p,\gamma\rangle G(T_9) \times\exp\left[\frac{-11.605Q}{T_9}\right] \tag{9}$$

with the reduced mass μ and the spin factor ω. Because the resonance levels decay predominantly to the first excited state at 0.09 MeV and only very weakly to the ground state of ^{32}Cl, the equation is weighted with a partition function $G(T_9)$ which takes the ground state branching and the population of the first excited state as a function of temperature into account. The comparison between these rates allows us to calculate the temperature and density conditions at which the proton capture dominates the depletion of ^{31}S and allows leakage out of the SiP-cycle. Figure 6 demonstrates these conditions (shaded area). The curves indicate the temperatures and

TABLE IV. Resonance parameters in $^{31}S(p,\gamma)^{32}Cl$.

E_x (keV)	$E_r^{c.m.}$ (MeV)	J^π	$\omega\gamma_{expt}$ (eV)	$\omega\gamma_{theo}$ (eV)
1735±3	0.162±11	3^+	$2.3^{+5.8}_{-1.7}\times10^{-10}$	$5.4^{+13.7}_{-4.1}\times10^{-10}$
2129±3	0.556±11	3^+	$5.5\pm1.2\times10^{-3}$	$4.4\pm0.2\times10^{-3}$
2213±3	0.640±11	1^+	$1.3\pm0.8\times10^{-2}$	$1.6\pm0.1\times10^{-2}$
2281±3	0.708±11	2^+	$3.5\pm0.6\times10^{-3}$	$2.5\pm0.1\times10^{-3}$

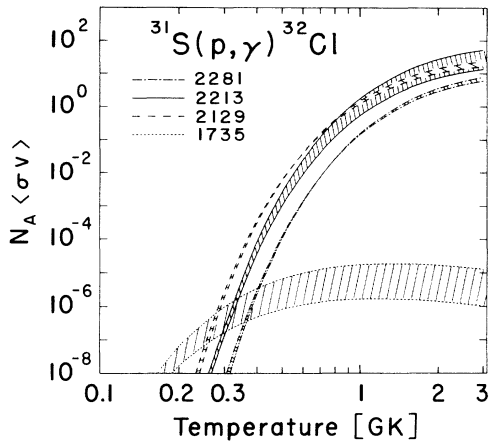

FIG. 4. The $^{31}S(p,\gamma)^{32}Cl$ resonant reaction rates as a function of temperature. The dashed areas reflect the uncertainty due to the uncertainty in level energy and partial width.

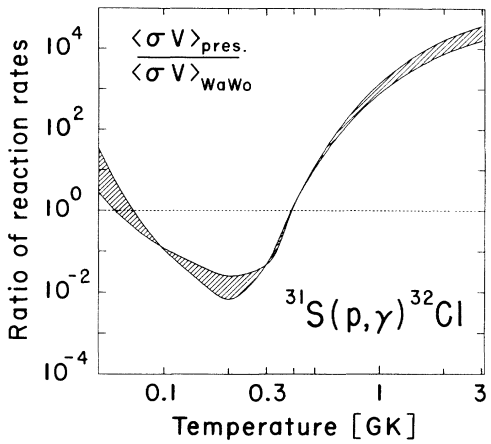

FIG. 5. Ratio of the present reaction rate of $^{31}S(p,\gamma)^{32}Cl$ and the previous rate by Wallace and Woosley (Ref. [1]) as a function of temperature. The dashed area reflects the uncertainty in the reaction rate ratio.

densities where the β decay and the proton capture of ^{31}S are of equal strength and where the proton capture on ^{31}S is equal to the inverse photodisintegration of ^{32}Cl. Because of the weakness of the resonances, the proton capture rate is small and the breakout occurs only at fairly high temperature and density conditions. For low temperatures the β-decay of ^{31}S is faster than the proton capture. At very high temperatures and lower densities the inverse photodisintegration substantially hinders the (p,γ) reaction flow.

To investigate the breakout from the SiP cycle in terms of the reaction flow and the influence of the isotopic abundances in this mass range, network calculations have been performed for different temperature and density conditions with an initial solar isotopic abundance distribution. The integrated reaction flow F_{ij} between two nuclei i,j is defined by the following expression

$$F_{ij} = \int \left[\frac{dY_i}{dt}(i \to j) - \frac{dY_j}{dt}(j \to i)\right] dt; \qquad (10)$$

$\frac{dY_i}{dt}(i \to j)$ is the change of the isotopic abundance Y_i ($Y = X/A$, mass fraction divided by atomic number) with time, induced by all reactions converting nucleus i to j. The total time evolution of the isotopic abundances is calculated from all depleting and producing reactions as a function of temperature and density,

$$\frac{dY_i}{dt} = \sum_j \lambda_j^i Y_j + \sum_{j,k} \lambda'_{jk} Y_j Y_k + \sum_{i,k,l} \lambda''_{jkl} Y_j Y_k Y_l. \qquad (11)$$

The first term in the equation includes β decays and photodisintegration of all nuclei j to i, or destroying i if $j = i$ ($\lambda^i < 0$); the second term describes two particle reaction processes between nuclei j and k leading to i or destroying i if either $j = i$ or $k = i$ ($\lambda'_{jk} < 0$) with $\lambda'_{jk} = 1/(1+\delta_{jk})N_A\rho\langle\sigma v\rangle_{jk}$; the third term describes the interaction between three particles j,k,l forming nucleus i or destroying i if $j = i, k = i$ or $l = i$ ($\lambda''_{jkl} < 0$) with $\lambda''_{jkl} =$

TABLE V. Recommended reaction rate for $^{31}S(p,\gamma)^{32}Cl$ in units of $\frac{cm^3}{moles}$.

	Resonance contributions				Total rate
T_9	162 keV	556 keV	640 keV	708 keV	$N_A\langle\sigma v\rangle$
0.06	6.21×10^{-17}	1.20×10^{-42}	2.56×10^{-49}	1.31×10^{-55}	6.21×10^{-17}
0.08	1.02×10^{-13}	3.70×10^{-31}	4.58×10^{-36}	6.29×10^{-41}	1.02×10^{-13}
0.10	8.00×10^{-12}	2.68×10^{-24}	3.80×10^{-28}	3.75×10^{-32}	8.00×10^{-12}
0.15	2.29×10^{-9}	3.20×10^{-15}	1.17×10^{-17}	1.60×10^{-20}	2.29×10^{-9}
0.20	3.42×10^{-8}	9.73×10^{-11}	1.80×10^{-12}	9.21×10^{-15}	3.43×10^{-8}
0.25	1.60×10^{-7}	4.42×10^{-8}	2.17×10^{-9}	2.44×10^{-11}	2.07×10^{-7}
0.30	4.27×10^{-7}	2.48×10^{-6}	2.33×10^{-7}	4.44×10^{-9}	3.15×10^{-6}
0.40	1.33×10^{-6}	3.49×10^{-4}	7.38×10^{-5}	2.71×10^{-6}	4.26×10^{-4}
0.60	3.47×10^{-6}	4.11×10^{-2}	1.95×10^{-2}	1.39×10^{-3}	6.20×10^{-2}
0.80	4.93×10^{-6}	3.92×10^{-1}	2.81×10^{-1}	2.77×10^{-2}	7.01×10^{-1}
1.00	5.64×10^{-6}	1.41	1.29	1.54×10^{-1}	2.85
1.50	5.75×10^{-6}	6.59	8.33	1.30	$1.62\times10^{+1}$
2.00	5.11×10^{-6}	$1.25\times10^{+1}$	$1.87\times10^{+1}$	3.32	$3.45\times10^{+1}$
3.00	3.80×10^{-6}	$2.00\times10^{+1}$	$3.50\times10^{+1}$	7.11	$6.21\times10^{+1}$

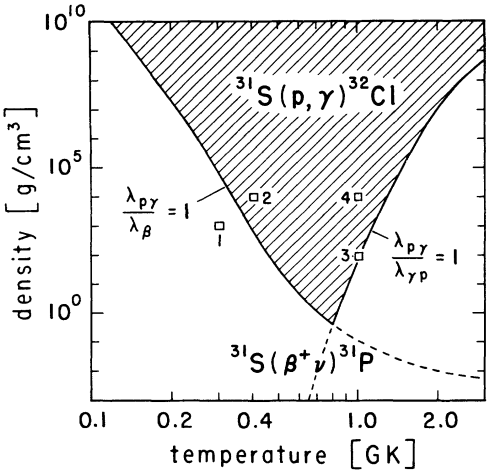

FIG. 6. Density and temperature boundary for a breakout from the SiP cycle, initiated by the $^{31}S(p,\gamma)^{32}Cl$ reaction. The shaded area represents the conditions where a continuous rp-process reaction flow will bypass the SiP cycle. The unshaded area represents the temperature and density conditions at which ^{31}S will predominantly β decay. Also indicated are the temperature and density conditions where flow and abundances are discussed in more detail.

$(1+\delta_{jk}+\delta_{jl})/(1+\delta_{jk}+\delta_{jl}+\delta_{kl}+2\delta_{jkl})N_A^2\rho^2\langle\sigma v\rangle_{jkl}$. Details of the network have been described earlier [7,22].

Figure 7 shows the reaction flow in the Si to Ar mass range calculated for four different temperature and density conditions, indicated in Fig. 6, to demonstrate the formation and the leakage of a SiP cycle. Figure 7(a) indicates the flux for a fairly low temperature and density scenario typical for novae [23], $T = 3\times10^8$ K, $\rho = 10^3$ g/cm^2; at these conditions, the SiP-cycle operates with no leakage via the $^{31}S(p,\gamma)$ reaction but some via the $^{31}P(p,\gamma)$ reaction [5,6]. Figure 7(b) shows the flux at temperature and density conditions, $T = 4\times10^8$ K, $\rho = 10^4$ g/cm^2. The flow pattern is characterized by a continuous rp-process flux because a considerable leak from the SiP-cycle occurs via $^{31}S(p,\gamma)$ (see also Fig. 6). For high temperature, low density scenarios as expected in Thorne-Zytkow objects [24], $T = 10^9$ K, $\rho = 10^2$ g/cm^2, however, the cyclic flow pattern reemerges again [Fig. 7(c)] because the large $^{31}S(p,\gamma)$ rate is considerably reduced by the inverse photodisintegration rate (Fig. 6). For higher densities anticipated in x-ray burst events [25], $\rho = 10^4$ g/cm^3, the flow again bypasses the SiP cycle [Fig. 7(d)].

The isotopic abundances in the Si-S mass range have been calculated as a function of time to study the impedance effect of the SiP cycle on the rp-process reaction flow. Figure 8 shows the abundances of ^{28}Si, ^{30}S, ^{31}S, and ^{32}S calculated for the same temperature and density conditions as in Fig. 7. At low temperature and density conditions [Fig. 8(a)] the initial ^{28}Si is quickly depleted after $\approx$1 s but the material remains stored mainly as ^{30}S and ^{31}S within the SiP cycle. The main leakage to ^{32}S occurs via the $^{31}P(p,\gamma)$ reaction. This limits the storage time in the cycle to $\tau \approx 7.7$ s [see Eq. (2)]. This time is comparable with the process time $\tau_{tot} \approx 8.8$ s for a sequential rp-process triggered by the initial ^{20}Ne abundance. At these conditions the time scale for the sequential process and the storage time in the cycle are of the same order of magnitude. This already indicates a significant delay for the continuous nucleosynthesis process within the short timescales of the explosive event. Depending on these time scales, this delay may inhibit further processing of the material towards heavier masses.

For the conditions represented in Fig. 8(b), the cycle is essentially open, the initial abundance is converted to ^{30}S. The storage time in this mass region corresponds essentially to the lifetimes of the β-unstable isotopes along the reaction path, $\tau_{cyc} \approx \tau_\beta(^{30}S) = 1.7$ s. After the decay of these isotopes the material is processed further via

$$^{30}S(\beta^+\nu)^{30}P(p,\gamma)^{31}S(p,\gamma)$$

towards the mass $A = 40$ region.

For high temperature, low density conditions [Fig.

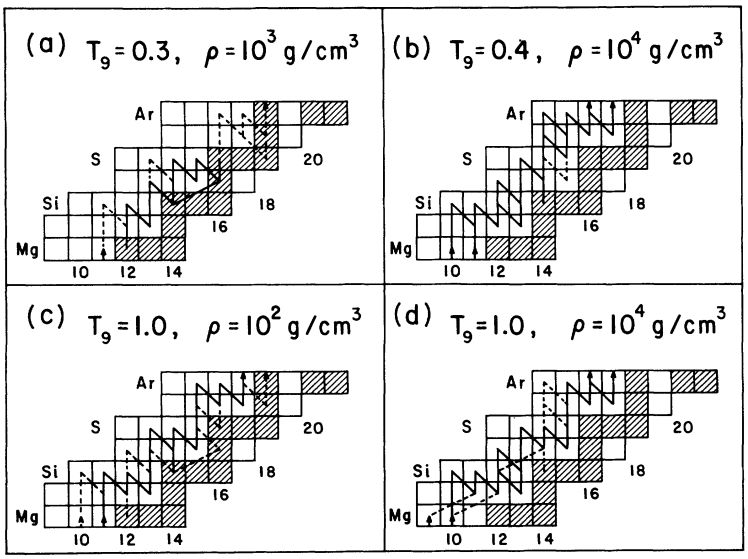

FIG. 7. Flow pattern of nuclear reactions in the mass range A=22–36 for different temperature and densities, calculated for a time period of $t = 10^3$ s. The connecting lines indicate the time integrated fluxes F_{ij} for reactions between nucleus i and j. The thick solid lines indicate a flux $F_{ij} \geq 0.1F_{max}$ with F_{max} as the maximum reaction flux at the particular temperature and density. The dashed lines indicate a flux $0.01F_{max} \geq F_{ij} < 0.1F_{max}$ and the dotted lines a small flux of $10^{-3}F_{max} \geq F_{ij} < 10^{-2}F_{max}$.

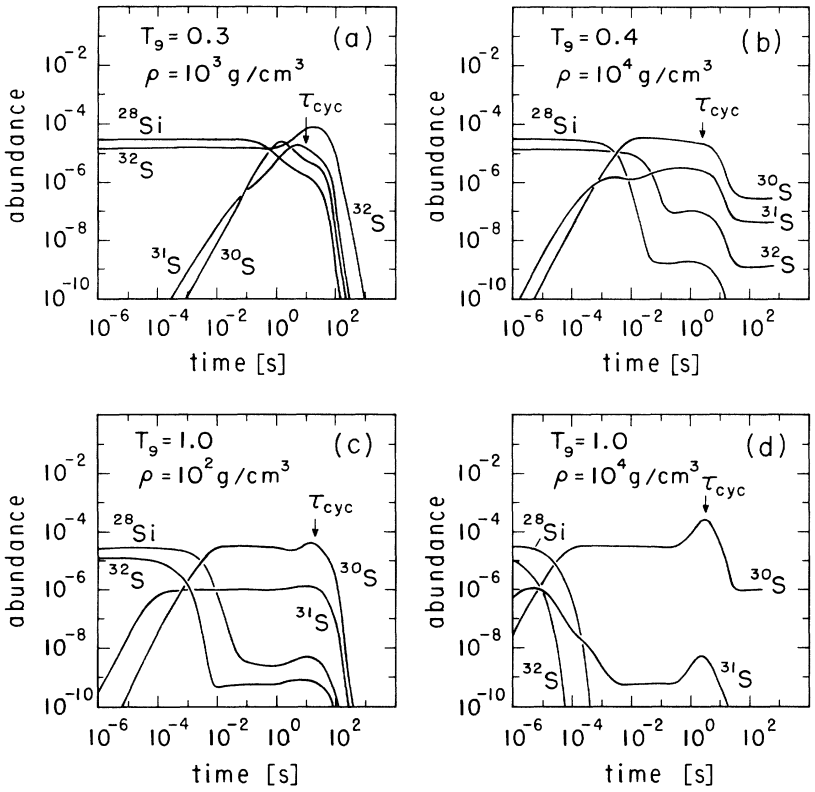

FIG. 8. Isotopic abundances of ^{28}Si, ^{30}S, ^{31}S, and ^{32}S plotted as a function of time for the temperature and density conditions marked in the previous figures. Also indicated are the respective lifetimes of the SiP cycle.

8(c)], however, the SiP cycle again is effective because of the reduced reaction rate for the breakout branch via ^{31}S(p,γ). The storage time in the cycle $\tau_{\rm cyc} \approx 18$ s represents a delay comparable to the total process time $\tau_{\rm tot} \approx 26$ s.

At higher densities [Fig. 8(d)] the cycle is open to leakage via the ^{31}S$(p,\gamma)^{32}$Cl reaction and presents essentially no impedance to the reaction flow in the low mass range ($A \leq 32$). Only under these conditions is a continuous fast rp-process towards the isotopes in the Fe-Ni range guaranteed. The time scale is entirely determined by the lifetimes of the β-unstable waiting point isotopes, like ^{30}S, along the reaction path.

The present network calculations for static temperature and density conditions give a qualitative picture about the reaction flow in explosive hydrogen burning in the Si, P, S mass range. This allows one to determine the temperature and density conditions at which the ^{31}S$(p,\gamma)^{32}$Cl reaction is of importance for nucleosynthesis in the SiP cycle. Such conditions are reached in novae, supernovae shock fronts, and Thorne-Zytkow stars (for details see Ref. [22]) for time scales comparable to the nuclear time scales discussed in the present work. Therefore, a fully dynamical treatment is necessary for quantitative predictions for the nucleosynthesis and energy generation in these scenarios.

ACKNOWLEDGMENTS

The authors wish to thank F.-K. Thielemann for many helpful discussions. This work was supported by the U.S. National Science Foundation Grants Nos. PHY 88-03035 and PHY 91-00708.

[1] W.K. Wallace and S.E. Woosley, Astrophys. J. Suppl. Ser. **45**, 389 (1981).
[2] A.E. Champagne and M. Wiescher, Annu. Rev. Nucl. Part. Sci. **42**, 39 (1992).
[3] J. Görres, M. Wiescher, and C. Rolfs, Astrophys. J. **343**, 365 (1989).
[4] R. Timmermann, H.W. Becker, C. Rolfs, U. Schröder, and H.P. Trautvetter, Nucl. Phys. **A477**, 105 (1988).
[5] C. Iliadis, U. Giesen, J. Görres, S. Graff, M. Wiescher, R.E. Azuma, M. Buckby, J. King, C.A. Barnes, and T.R. Wang, Nucl. Phys. **A533**, 153 (1991).
[6] C. Iliadis, J. Görres, J.G. Ross, K.W. Scheller, M. Wiescher, C. Grama, Th. Schange, H.P. Trautvetter, and H.C. Ewans, Nucl. Phys. **A559**, 83 (1993).
[7] M. Wiescher, J. Görres, F.-K. Thielemann, and H. Ritter, Astron. Astrophys. **160**, 156 (1986).
[8] M.A.J. Snijders, T.J. Batt, P.F. Roche, M.J. Seaton, D.C. Morton, T.A.T. Spoelstra, and J.C. Blades, Mon. Not. R. Astron. Soc. **228**, 329 (1987).
[9] P. Saizar, S. Starrfield, G.J. Ferland, R.M. Wagner, J.W. Truran, S.J. Kenyon, W.M. Sparks, R.E. Williams, and L.L. Stryker, Astrophys. J. **398**, 398 (1992).

[10] S. Starrfield, S.N. Shore, W.M. Sparks, G. Sonneborn, J.W. Truran, and M. Politano, Astrophys. J. **391**, L71 (1992).
[11] S. Starrfield, J.W. Truran, M. Politano, W.M. Sparks, I. Nofar, and G. Shaviv, Phys. Rep. **227**, 223 (1993).
[12] C. Jeanperrin, L.H. Rosier, B. Ramstein, and E.I. Obiajunwa, Nucl. Phys. **A503**, 77 (1989).
[13] T. Björnstad, M.J.G. Borge, P. Dessagne, R.-D. von Dincklage, G.T. Ewan, P.G. Hansen, A. Huck, B. Jonson, G. Klotz, A. Knipper, P.O. Larson, G. Nyman, H.L. Ravn, C. Richard-Serre, K. Riisager, D. Schardt, and G. Walter, Nucl. Phys. **A443**, 283 (1985).
[14] D. Schardt and K. Riisager, in *Nuclei far from Stability*, Proceedings of the Sixth International Conference on Nuclei Far from Stability, edited by R. Neugart and A. Wöhr, IOP Conf. Proc. No. 132 (Institute of Physics and Physical Society, London, 1992), p. 805; GSI Report No. GSI 93-05.
[15] D. Schardt, private communication.
[16] J.D. Goss, A.A. Rollefson, and C.P. Browne, Nucl. Instrum. Methods **109**, 13 (1973).
[17] L.K. Fifield and P.M. Orr, Nucl. Instrum. Methods Phys. Res. Sect. A **288**, 360 (1990).
[18] L.O. Lamm, S.M. Graff, M. Wiescher, J. Görres, C.P. Browne, and U. Giesen, Nucl. Instrum. Methods Phys. Res. Sect. A **281**, 143 (1989).
[19] P.M. Endt, Nucl. Phys. **A521**, 1 (1990).
[20] B.A. Brown and B.H. Wildenthal, Nucl. Phys. **A474**, 290 (1987).
[21] W.A. Fowler, G.R. Caughlan, and B.A. Zimmerman, Annu. Rev. Astron. Astrophys. **5**, 525 (1967).
[22] L. van Wormer, J. Görres, C. Iliadis, M. Wiescher, and F.-K. Thielemann, Astrophys. J. (in press).
[23] J.W. Truran, in *Physics of Classical Novae*, edited by A. Cassatella and R. Viotti, Lecture Notes in Physics Vol. 369, (Springer-Verlag, Berlin, 1990), p. 373.
[24] G.T. Biehle, Astrophys. J. **380**, 167 (1991).
[25] R.E. Taam, Annu. Rev. Nucl. Sci. **35**, 1 (1985).